Ab-initio studies of the optoelectronic structure of undoped and doped silicon nanocrystals and nanowires. Role of size, passivation, symmetry and phase

Stefano Ossicini,*[ab] Ivan Marri,[b] Michele Amato,[c] Maurizia Palummo,[d] Enric Canadell,[e] and Riccardo Rurali,[e]

Silicon nanocrystals and nanowires have been extensively studied because of their novel proper-ties and their applications in electronic, optoelectronic, photovoltaic, thermoelectric and biological devices. Here we discuss results of ab-initio calculations for undoped and doped Si nanocrystals and nanowires showing how theory can aid and improve the comprehension of the structural, electronic and optical properties of these systems.

1 Introduction

The scaling down of Si structures to nanometer size has opened new chances to overcome the inability of bulk Si as efficient light emitter. In low-dimensional Si-based nanosystems, such as porous-Si (a quantum sponge made up of Si nanostructures), Si nanowires (Si-NWs) and Si-nanocrystals (Si-NCs), the possibility to achieve efficient visible photoluminescence (PL) has been clearly demonstrated [1–7]. In these nanostructures the low-dimensionality causes the zone folding of the conduction band minimum of bulk Si, thus introducing a quasi-direct band gap. Furthermore, the quantum confinement (QC) effect induced by size and dimensionality reduction of the systems enlarges the energy band gap enabling light emission in the visible range [8]. QC can also enhance the spatial localization of electron and hole wave functions and their overlap, and thus the probability of their recombination. Moreover, size reduction offers the possibility to modulate the electronic and optical properties and therefore to increase the solar light harvesting, opening new routes in the development of efficient, nanostructured, Si-based solar cell devices [9].

Si-NCs have attracted, from the beginning, much interest because they exhibit very bright visible PL, which is tunable with respect to their dimensions, and sample dependent high quantum yields, that can be enhanced by careful surface passivation [10]. Optical gain in Si-NCs has been observed and studied [11–14], multiple exciton generation effects in excited carrier dynamics after the absorption of a single high-energy photon have been proved in ensemble of Si-NCs, revealing an efficient carrier photogeneration that could increase solar cell performances [15–22]. Indeed a full exploitation of size, shape and surface termination [23–32] of Si-NCs together with their low toxicity and good bio-compatibility has boosted their application in microeletronics [33–36], photonics [37–39], non-linear optics [40], photovoltaics [9,41,42], thermoelectrics [43] , nano and biomedicine [44–49].

Si-NWs are particularly appealing thanks to bottom-up growth, that allows at overcoming the limit of conventional lithography based top-down design. Si-NWs with very small diameters (of the order of few nm) have been successfully grown and several applications have been demonstrated in the field of electronics devices, nonvolatile memories, photonics, photovoltaics, biological sensors and thermoelectrics [5,50–52]. In particular in these one-dimensional structures the electronic and optical properties strongly depends not only on the diameter, but also on the growth orientation, the surface termination and on the crystal phase [53,54].

An additional degree of freedom in semiconductor materials design is given by the introduction of impurities. Controlled doping is at the heart of the modern Si-based semiconductor industry. The presence of the dopants changes remarkably the optical and electronic properties of the host material. In particular, B and P impurities introduce very shallow levels in the band gap of bulk Si (above the valence band and below the conduction band, respectively) than can be efficiently ionized at room temperature increasing dramatically the conductivity of bulk Si. Doping in Si nanostructures can be used to alter in a controllable way the electronic, optical and transport properties of nanomaterials. As a consequence, intentional doping with n- and p-type impurities can be exploited to design and realize novel devices. The possibil-

[a] *Dipartimento di Scienze e Metodi dell'Ingegneria, Centro Interdipartimentale En&Tech, Universitá di Modena e Reggio Emilia, Via Amendola 2 Pad. Morselli, I-42125 Reggio Emilia; E-mail: stefano.ossicini@unimore.it*

[b] *"Centro S^3", CNR-Istituto di Nanoscienze, Via Campi 213/A, I-41125 Modena, Italy.*

[c] *Laboratoire de Physique des Solides (LPS), CNRS, Université Paris Sud, Université Paris-Saclay, Centre Scientifique d'Orsay, F91405, Orsay cedex, France.*

[d] *.Dipartimento di Fisica and INFN, Universitá di Roma Tor Vergata, Via della Ricerca Scientifica 1, 00133 Roma, Italy.*

[e] *Institut de Ciéncia de Materials de Barcelona (ICMAB-CSIC), Campus de Bellaterra, 08193 Bellaterra, Barcelona, Spain.*

ity of enhancing the electrical conductivity of nanosized systems has been attempted, for instance, by fabricating porous-Si from n- or p-doped bulk Si by means of an electrochemical etching[55]. However, though the etching process does not remove the impurities from the system[56], a very low conductivity was measured, even for the larger mesoporous samples. This suggests that the ionization of the impurities at room temperature may be strongly quenched with respect to the bulk. Therefore the possibility of generating free charge carriers from impurity states can be limited by size effects. As for the optical properties, the introduction in Si nanostructures of an isoelectronic impurity can modify the indirect nature of band gap in bulk Si. However, Si does not possess proper isoelectronic impurities that can strongly localize excitons at room temperature and enhance the PL intensity. An alternative approach is given by codoping. i.e. the formation of Si nanosystems with the same number of n- and p-type impurities[57]. The first attempts to dope Si nanostructures started about two decades ago. The results obtained revealed that doped Si nanostructures showed different properties with respect to the doped Si-bulk[58–60].

From an experimental point of view, several factors contribute to make the interpretation of the measurements on these systems a difficult task. First of all, independently on the fabrication technique, the degree of reproducibility of a single individual NC is very low. For instance, samples show a strong dispersion in the Si-NC size, that is difficult to determine. In this case it is possible that the measured quantity does not correspond exactly to the mean size but instead to the most responsive Si-NCs[61]. Moreover, Si-NCs synthesized by different techniques often show different properties in terms of size, shape and in the structure of the interface. Finally, in solid nanocrystal arrays, some collective effects caused by electron, photon, and phonon transfer between Si-NCs can render more complicated the interpretation of the experimental results.

In this context the role of theoretical modeling and simulations is extraordinarily important. In particular, ab-initio approaches represent a unique and very powerful instrument to predict and design the properties of novel molecules, materials, and devices with an accuracy that complements the experimental characterization. Thus the importance of the theoretical investigation lies not only in the interpretation of the experimental results but also in the possibility to predict structural, electronic, optical and transport properties of unexplored materials.

In this work we will describe recent and new results obtained by ab-initio simulations for doped and codoped Si-NCs and Si-NWs. We will mainly consider B and P as dopant atoms due to their high solid solubility in silicon and because they are the most commonly used impurities at experimental level. The whole discussion will be conducted taking as reference the corresponding results for undoped nanostrutures to underline the differences and novelties introduced by the presence of impurities. In particular, together with previous outcomes, we will present new results related to the doping of Si nanocrystals with different group-III and group-V species, to the band structures of cubic Si-NWs and to the comparison for stability and segregation of several dopants in cubic and hexagonal Si-NWs. It is worthwhile to note that new calculations have been explicitly performed in order to achieve a better comparison with respect to previous results obtained through the use of several computational packages. In particular we note that different codes applied to the same nanosystem calculate energy eigenvalues that differ less than 0.05 eV.

The paper is organized in the following way: in section 2 we briefly describe the ab-initio models used for the calculations of the structural, electronic and optical properties of Si nanostructures. In section 3 we present results regarding free-standing and matrix-embedded Si-NCs, with particular focus on the theoretical calculations for undoped (see subsections 3.1) and doped NCs. We will consider mainly B and P impurities (see subsections 3.2), but a section has been devoted to other p- and n-doping atomic species (see subsections 3.3). Section 4 instead is devoted to Si-NWs, with a subsection dedicated to the theoretical results for NWs with different phases (subsection 4.3). Conclusions are presented in section 5.

2 Computational methods

Computational modelling of the structural, electronic and optical properties of complex systems is nowadays accessible, thanks to the impressive development of both theoretical approaches and computing facilities. Surfaces, interfaces, nanostructures, and even biological systems can now be studied within ab-initio methods. Even within the Born-Oppenheimer approximation, which allows at decoupling the ionic and electronic dynamic, the solution of the Schrödinger equation that governs the physics of all those systems is a formidable task due to the many-body long-range electronic coulomb interaction. It is hence necessary to resort to further approximations. Density Functional Theory (DFT) avoids dealing directly with the Many-Body equation by mapping the interacting system into a fictitious non-interacting system, which is then described by self-consistent single particle equations[62,63]. Despite DFT is a ground state theory based on relations that represent a fictitious auxiliary system with no physical meaning, it is often used to calculate band structures and their eigenvalues are often interpreted as one electron excitation energies corresponding to the excitation spectra of the system upon removal or addition of an electron. The level of accuracy is often related to the approximation used to describe the exchange correlation energy (Exc). Here we adopt the Local Density Approximation (LDA) where Exc of the system is replaced with the one of a uniform electron gas with the same density. DFT-LDA is computationally cheap and permits to investigate systems of realistic size, the agreement with experiments is often remarkable, but sometimes only qualitative: the electronic gaps of semiconductors are, as a matter of fact, always systematically underestimated within DFT. The Green's function approach should be the formally correct approach to obtain the electronic addition and removal energies, through the solution of the so-called quasi-particle (QP) equation. This is formally similar to the KS equation but instead of the exchange-correlation potential a non-local, energy dependent and non-hermitian self-energy (usually estimated within the GW approximation) operator appears. This physically means that excitations are described are described in terms of a particle of finite life time, that represent the extra electron (and/or the extra

hole added to the system) plus its screened interaction with the electrons of the system[64]. Nevertheless, due to the complexity and high-computational cost of solving this QP equation, what is usually done is to estimate in a perturbative way, the exchange correlation potential, V_{xc}, and correct the KS energies. To resolve this problem on can use, on top of DFT-LDA, the Green's function approach (in the so called GW approximation), that maps the Many-Body electronic problem to a system of quasi-particles. The main consequence of adopting this approach is the opening of the band gap by amounts that, for nanostructures, are strongly size dependent.

As for the optical properties, one can perform first-principles calculation of the dielectric response taking into account many-body interaction (namely excitonic and local-field effects) through the solution of the Bethe-Salpeter equation (BSE)[65] always within the Many-Body Green's function approach. However, it is worth noting that results obtained through LDA are still interesting for several reasons: i) the inclusion of many-body effects is computationally very demanding and thus limited to small nanocrystals and nanowires[53,66,67], ii) an almost complete compensation of self-energy and excitonic effect[68–70] has been observed in silicon based nanostructures, thus rendering the KS based description significant, iii) very often, one is interested in trends of a specific property whose behaviour remains similar going from independent-particle approximation to the many-particle corrections. Thus, when not stated otherwise, the results of this paper are mainly been obtained using the DFT-LDA approaches. In all the performed supercell calculations the optimized structures have been achieved by relaxing all atomic postions and cell parameters. Several different packages have been used, QUANTUM ESPRESSO[71,72], SIESTA[73], ABINIT[74], VASP[75] and YAMBO code[76].

3 Silicon nanocrystals

3.1 Undoped isolated and matrix embedded Si-NCs wih different passivation

Si-NCs have been largely investigated in the last two decades by scientific community for different technological applications. Research activities have been mainly focused on the study of microscopic properties of these systems, and in particular of the mechanisms that rules their electronic and optical properties. Despite the relevant efforts dedicated to the study of these systems, important issues remain unsolved. For instance, experiments have not totally clarified the microscopic origin of the PL peak in Si-NCs; sometime it was assigned to transition between states localized inside the Si-NC, other times to transition between defects and/or interface states[33]. In this context, theory can play a crucial role and can support experimental investigation by solving fundamental controversial. In order to investigate PL in Si-NCs, we have considered two different types of surface termination for our model. In the first case the dangling bonds at the surface of the Si-NCs are passivated with H atoms. Although Si-NCs usually experience oxidation, there are experiments where NC surface are passivated with H[77]. In the second case we have performed studies for the same Si-NCs, but now with dangling bonds capped by OH terminations. NCs have been always modelled by using a supercell method, where a large region of vacuum was adopted to separate points at the surface of the NC and its images, thus avoiding effects induced by spurious interactions between replicas. We consider both spherical-like and faceted Si-NCs. The first are obtained by cutting Si atoms outside a sphere from Si bulk, whereas the faceted NCs result from a shell-by-shell construction procedure, in which one starts from a central atom and adds shells of atoms successively. Figure 1 shows the obtained results for the Highest Occupied Molecular Orbital (HOMO)-Lowest Unoccupied Molecular Orbital (LUMO) gaps for both the hydrogenated and hydroxided Si-NCs. The investigation of the spatial localization of HOMO and LUMO for the Si-NCs passivated with H shows that these states are not related to H atoms. Therefore, the dependence of HOMO-LUMO gap on the Si-NCs diameter is a direct consequence of the QC effect (the NC shape does not have any influence) and thus the observed PL is directly related to states localized inside the Si-NCs[60,78–80]. For the OH-terminated Si-NCs, instead, the changes in the HOMO-LUMO gap are strongly dependent from the oxidation degree (see Table 1) at the NCs interface. Infact, in these NCs, the Si atoms at the interface have a different number of nearby O atoms. By defining an oxidation degree Ω as the ratio between the number of O atoms and the number of Si atoms bonded to them, we can compare the behavior of the HOMO-LUMO gap with the oxidation degree (see second and third columns of Table 1). What emerges is a strong correlation between the calculated gap values and Ω (a larger oxidation degree results in a larger gap), consequently the QC effect dependence from the size is still there (NCs with similar Ω show gaps with a clear dependence on the diameter), but strongly modulated by the presence of oxidation. It is worthwhile to note that a size-dependent experimental study of the Si core-level shifts for Si-NCs embedded in a SiO_2 matrix showed that the shell around the Si-NCs consists of three different Si suboxide states, where for NCs with diameter less than 3 nm the presence of suboxides with higher oxidation is favored[81].

Thus these results suggest that, in the case of Si-NCs embedded

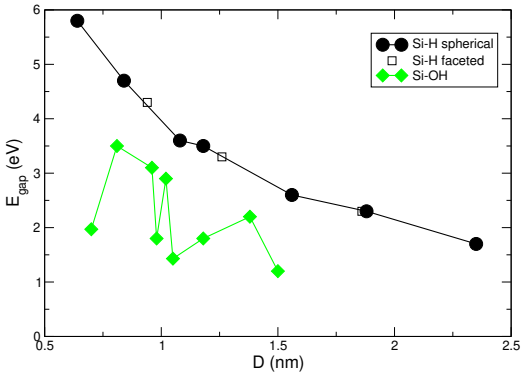

Fig. 1 HOMO-LUMO gaps for hydrogenated (black dots and black squares) and hydroxided (green diamonds) Si-NCs as function of the NC diameter.

Table 1 Energy gap (HOMO-LUMO) for the OH-terminated Si-NCs as function of the diameter and the oxidation degree Ω.

d (nm)	Ω	E_{gap}
0.70	1.6	1.97
0.81	3.0	3.50
0.96	3.0	3.05
0.98	1.5	1.89
1.02	2.8	2.93
1.05	1.2	1.50
1.18	2.0	1.83
1.38	3.0	2.26
1.50	1.46	1.19

in SiO_2 matrices, for diameters above a certain threshold, about 2-3 nm, the emission peak of the Si-NCs simply follows the QC model, while interface states assume a crucial role only for very small-sized Si-NCs[82–89].

3.2 Single B and P doped and codoped isolated and embedded Si-NCs

In bulk Si the level of doping lies in the interval 10^{13}-10^{18} cm^{-3}. In a Si-NC of about 2 nm in diameter, which possess more than 200 Si atoms, the introduction of a single impurity atom corresponds to a doping level of about 10^{20} cm^{-3}, that is a quite different situation. Despite the large number of works dedicated to the study of doped and codoped Si-NCs, important unsolved issues still exist. The effective dopant location, the occurrence of self-purification effects (the tendency of the Si-NC to expel the dopant atoms towards its surface), as well as the role played by the chemical environment of the Si-NCs are topics still under discussion[56,58,59,90–97].

In H-terminated Si-NCs the dopant atom could be either inside the NC or on a surface position. In order to define the most stable impurity location, we have probed all the possible substitutional sites, moving from the center of the Si-NC to the surface. For each configuration, calculations of formation energies (FE) have been performed. As is known, this is a crucial quantity that allows at understanding which is the energy cost of creating a defect into an host crystal[98–100]. The results for the FE show that the B neutral impurity tend to migrate towards a subsurface position, the position directly below the interface Si atoms linked to H. This is explained by considering that such positions are the only ones that allow a significant atomic relaxation around the impurity. For P impurities this behavior depend on the Si-NC diameter, in fact P atoms prefer to stay at the subsurface positions for Si-NCs with diameter less than 2 nm, whereas for larger nanocrystals the Si-NC center is the energetically most favorable position. These results are not only confirmed by several calculations[91,97,101], but also supported by experiments[102–104], thus confirming the possibility to incorporate B and P as impurities even in small Si-NCs[60].

Calculations on matrix-isolated single doped Si-NCs clearly indicate that for n-type doping the impurity tends to settle in the Si-NC core. Instead, in the case of p-type doping the interfacial sites are favored. Moreover, the doping of the SiO_2 region is unlikely to occur. In particular, a very high FE is required to move a P dopant from the Si-NC core to the silica[105]. This is in agreement

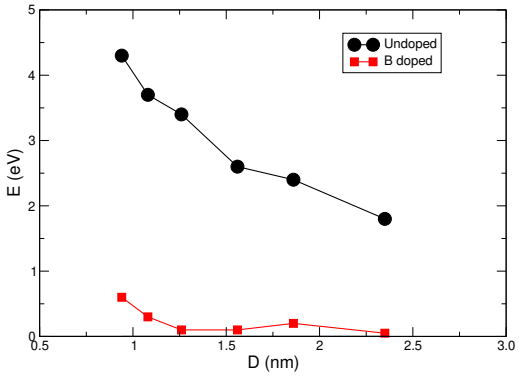

Fig. 2 Position in energy, with respect to the HOMO (set equal to zero), of the B related impurity state (red squares) and of the LUMO state for the undoped Si-NCs (black dots), as function of the NC diameter.

with the observation that for Si-NCs embedded in a SiO_2 matrix, the matrix provides a strong barrier to P diffusion, inducing P segregation in the Si rich region[106,107]. By contrast, still consistently with experiments[108], the diffusion of B toward the matrix is significantly easier. Once more the structural relaxation around the impurity plays a significant role. P atoms maintain a sort of tetrahedral coordination in all the cases, with all the bonds showing approximately constant characteristic lengths with Si and/or O. Instead, B atoms tend to form, when placed at the interface with two O atoms, a strong antibonding with one of the neighbors, causing repulsion to a large distance. Experimental results based on atom probe tomography and proximity histograms support these conclusions[109–111]

As regards as the electronic and optical properties for B and P single doped Si-NCs one has to consider that in Si bulk the extra hole associated to the B impurity creates an acceptor level slightly above, in energy, the valence band maximum, whereas for P impurity the extra electron creates a donor state slightly below the conduction band minimum. Figures 2 and 3 show our results for the position in energy of the calculated impurity state for the H-Si-NCs single doped with B (red squares) or P (green squares). The position of these impurity levels is compared with the energy of the LUMO for the undoped NCs. In both figures the zero in energy is set to the HOMO level of the corresponding undoped Si-NCs. The binding energy (BE) of the acceptor is defined as the energy difference between the impurity level and the HOMO, whereas the BE of the donor is given by the energy difference between the LUMO and the impurity level. Looking at the plots, it is clear that the BE strongly depend on NC size. On going to smaller NCs, the impurity levels, differently from the bulk case, are localized well inside the Si band gap and thus necessitate of a larger activation energy. As a consequence, the optical properties for single-doped Si-NCs show intense absorption peaks, due to transitions that involve the impurity states in the absorption. Only for the larger NCs (diameters of the order of 3 nm) the absorption spectra of the single doped case are very similar to that of the undoped case[60,80].

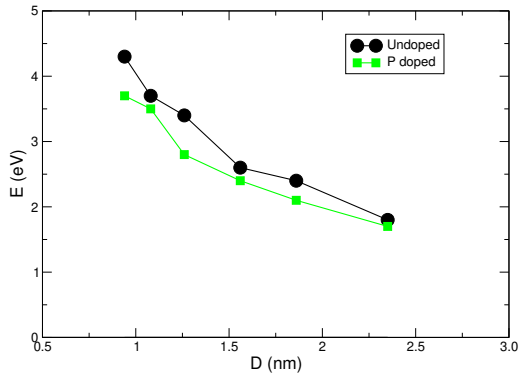

Fig. 3 Position in energy, with respect to the HOMO (set equal to zero), of the P related impurity state (green squares) and of the LUMO state for the undoped Si-NCs (black dots), as function of the NC diameter.

In the case of B and P codoped NCs the simultaneous doping strongly reduces the FE with respect to both B or P single doped cases, independently from their size[66,92]. This reduction is a consequence of the carriers compensation in codoped Si-NCs, that recover, around the impurities, an almost T_d configurations. Furthermore, the FE of the codoped Si-NCs depends on the distance between the two impurities. A reduction of the distance between the two impurities results in a reduction of the FE. In particular, the minimum of the FE is obtained when the impurities are located at the nearest neighbors locations at the surface of the Si-NCs. Noteworthy, it has been observed that codoping is an effective mean for promoting segregation and stability of the B and P impurities in the Si-NC interface region[109]. The fact that Si-NCs can be more easily codoped than single-doped explains the possibility of easily grow[57,112] B and P codoped colloidal Si-NCs.

As for the optoelectronic properties, Fig. 4 show our calculated energy gaps for B and P codoped Si-NCs in comparison with the calculated gaps for the corresponding undoped cases. We see the codoping originate a true lower energy gap. As shown in the inset of Fig. 4, this is due to the presence of both an acceptor (now fully occupied, localized on the B atom) and a donor state (now empty, localized on the P atom) within the undoped Si-NC band gap. In the codoped case the PL emission is thus originated from donor-acceptor pair recombination mechanism. This mechanism is at the origin of the possibility to tune the PL in codoped Si-NCs. This tuning has been experimentally observed and clearly related to the presence of donor-acceptor pair recombination[113–117]. Noteworthy, as consequence of donor-acceptor pair recombination, evidence of carrier multiplication in codoped Si-NCs has been reported[114].

3.3 Other group-III and group-V dopants

As previously underlined there are several difficulties concerning impurity doping in Si-NCs, i.e. self-purification effects, large impurity formation energies, difficulty in tracking the locations of dopants elements. Thus, while the doping of Si-NCs with boron and phosphorus has been studied in detail, the doping with other group-III and group-V species has been investigated in very few cases. To our knowledge there are no experimental works regarding other group-III elements, whereas for group-V dopants, with the exception of a study concerning the role of nitrogen in the formation of matrix-embedded Si-NCs[118], only arsenic has attracted some interest. In particular the structural and optical properties of As-doped Si-NCs embedded in silicon dioxide matrices have been investigated using Rutherford Backscattering Spectrometry, Transmission Electron Microscopy and Photoluminescence[119,120] and very recently using atom probe tomography[121]. It turns out that As show a similar behavior to phosphorus both regarding PL and the efficient incorporation of impurities in the core of Si-NCs. In this section we briefly present results of ab initio simulations concerning formation energies, changes in the structural features, atomic location and optical properties, in the case of Al (group-III) and N and As (group-V) doped Si-NCs, comparing the obtained trends with those for the B and P doped nanocrystals of the same size. All these new calculations have been performed for free standing Si-NCs caped by hydrogen atoms with the impurity located at the center of the NCs, whereas for the case of Si-NCs embedded in a SiO_2 matrix we have varied the atomic position of the doping species.

The calculated formation energies are similar for the case of group-III dopants (Al vs B), whereas in the case of group-V dopants they are larger for N with respect to P and As. This is a consequence of the larger rearrangement of the Si atoms near the impurity for the N case, owing to the small dimension of N. It is interesting to note that for Al impurity, as in the case of B, we found around the dopant a C_{3V} symmetry, due to the presence of one longer and three equally shorter Si-impurity distances, whereas in the case of As and P we found four similar impurity-Si bond lengths. The case of N represents again an exception, since the similarity between the four impurity-Si bond lengths is not so clear. Thus it seems that the structural features induced by the impurity presence are linked directly to the their valence (trivalent vs. pentavalent atoms). In the case of Si-NCs embedded in a silicon dioxide matrix, again, for p-type doping the behavior of Al is similar to that of B (the sites at the interface with the matrix are favoured), and for n-type doping the behavior of N is similar to that of P (there is for the impurity a strong tendency to be located in the Si-NC core).

Concerning the computed optoelectronic properties, the Al impurity (like B) originates shallow acceptor levels in the band gap of the Si-NCs, whereas N, differently from P, induces deep donor levels. Moreover, as consequence of the quantum confinement effect the energy position of these levels strongly depends on the Si-NCs diameter. For smaller diameters the acceptor and donor levels are located deeper in the nanocrystals band gap. Regarding the calculated optical spectra, in small Si-NCs the Al-related absorption peaks are more intense than those related to B impurity, but they become of similar intensity for larger nanocrystals. For group-V impurities the deeper donor character of the N impurity is clearly reflected in the optical spectra, that show impurity-related absorption peaks highest in energy with respect to the other dopants.

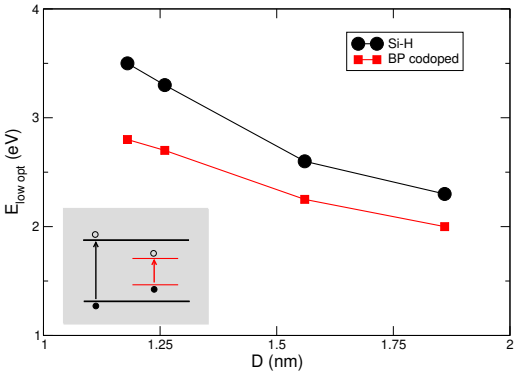

Fig. 4 Comparison between the HOMO-LUMO gaps of the undoped (black dots) and codoped (red squares) hydrogenated Si-NCs as a function of the NC diameter. In the inset a schematic illustration of the energy level structures in both cases.

4 Silicon nanowires

4.1 Cubic-diamond Si nanowires

Because of their natural compatibility with silicon based technologies, cubic-diamond (3C) Si-NWs have being extensively theoretically studied and several experiments have already characterized their main structural and electronic properties[5,6,50–52,54,122]. It has been possible to fabricate, for example, single-crystal Si-NWs with diameter as small as 1 nm and lengths of a few tens of micrometers. Ultrathin NWs show a substantial blue-shift with decreasing the size as revealed by STS measurements[123]. Si-NWs grow along well-defined crystalline directions: depending on the size, one can fabricate <110>, <111> and <112> NWs. In particular, surface passivation is required to obtain semiconducting ultrathin NWs.

Fig. 5 report our DFT-LDA calculations for the band structures of Si-NWs of different orientation and size. All the dangling bonds at the NW surface are capped by H atoms. We note that i) in all cases we find a direct band gap at Γ. The direct nature of the fundamental gap is due to the folding of bulk bands, ii) moreover, as consequence of QC effects, the electronics gaps are much larger with respect to bulk Si, iii) the electronic properties vary changing the growth orientation of wires. This is a result of the anisotropic behaviour of these low dimensional systems. Indeed the gap for the <100> direction is larger than that of <111> and <110> direction.

As regards the optoelectronic properties, we found that the GW correction the to DFT-LDA band gaps are much larger than in the bulk case and that they depend on the size and on the orientation of the wire. The excitonic effects are very strong originating a very large binding energy for the electron-hole bound states. Indeed the wires are almost transparent when the light is polarized in the direction perpendicular to the axis of the wire[53]. This is due to the microscopic fields, induced by the external perturbation, which screens the electric field in the NWs.

Table 2 reports our calculated DFT-LDA, quasi- particle (self-

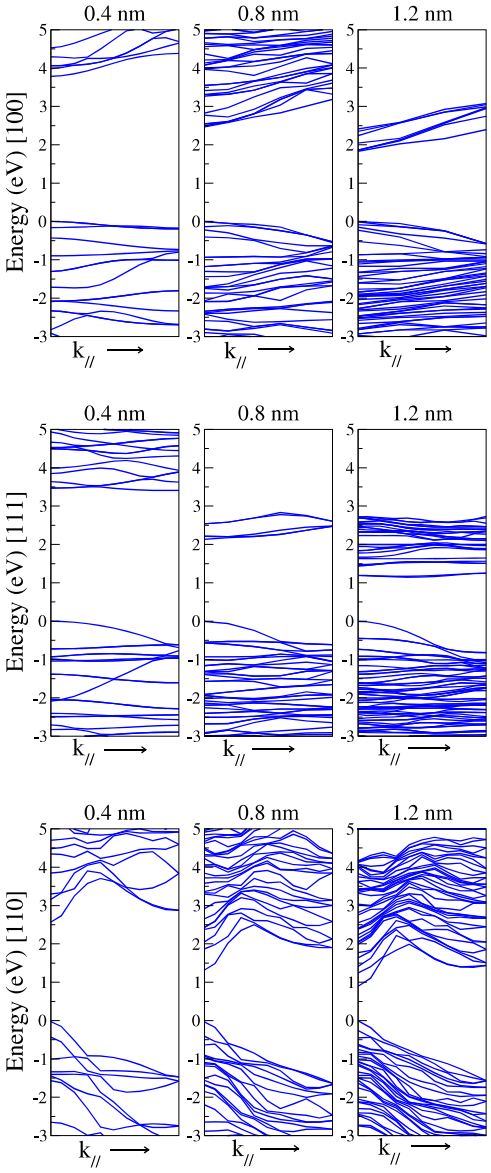

Fig. 5 Band structure at the DFT-LDA level for Si-NWs grown along the [100] (top panel), [111] (central panel), [110] (lower panel) direction. In each panel the plots for different wire cross section, l = 0.4 nm (left), l = 0.8 nm (center), l = 1.2 nm (right) are reported. The zero of the energy is set to the top of the valence band.

energy, GW calculations) and excitonic (BSE calculations) gaps for all the Si-NWs of Fig. 5. An almost complete compensation, for the absorption onset, of the self-energy and excitonic contributions is observed. This fact confirms again the validity of the DFT-LDA description, especially regarding trends of a specific quantity.

Table 2 DFT, quasi Particle and excitonic gaps for Si-NWs with different orientation and size. All values are in eV.

Wire size	Orientation	E_{gap}(DFT)	E_{gap}(QP)	E_{gap}(EXC)
	[100]	3.8	6.2	4.4
0.4 nm	[111]	3.5	5.7	4.1
	[110]	2.5	4.2	3.0
	[100]	2.5	4.2	3.0
0.8 nm	[111]	2.2	3.5	2.7
	[110]	1.4	3.0	1.8
	[100]	1.8	3.1	2.3
1.2 nm	[111]	1.2	2.3	1.9
	[110]	1.0	2.1	1.7

4.2 Doped cubic-diamond Si nanowires

Doping in 3C-Si-NWs has been examined in depth from theoretical and experimental point of view [124–136], focusing mainly on B and P single doping. Experimentally, it has been clearly demonstrated that, with the current growth methods, it is possible to incorporate group III and V impurities into the wire and to obtain both n-type and p-type wires. On the other hand, theoretical investigations have shown that B and P impurities give rise to energetic levels deep in the band gap, and that they prefer to segregate towards the surface of the wire in order to minimize mechanical stress and distortions. The simultaneous addition of B and P impurities, codoping, has also been demonstrated to be a fundamental tool for modifyng the electronic and optical features of NWs [137]. Unlike the case of B and P single doped systems, very few theoretical studies [124,130] have addressed the analysis of B and P codoped Si-NWs, and moreover they have been mainly focused on very thin NWs (with diameters up to 1.6 nm). We investigated the FE and the band structure for <110> oriented B-P codoped H terminated Si-NWs with a diameter of 2.4 nm using the SIESTA code [138]. The results show that the impurities tend to get closer together and to occupy edge positions, as a consequence of greater freedom of mechanical relaxations. P atoms will have a preference to sit in inner subsurface sites (as in the case of codoped Si-NCs). The simultaneous addition of B and P only slightly modifies the energy band gap value with respect to the pure wire (see Table 3) and the introduction of impurities does not change too much the dispersion of the electronic states. The analysis of wave function localization of the band edges shows that the top of the valence band is located at the B impurity, while the bottom of the conduction band is located at P. The calculated reduction of the band gaps is thus due to donor-acceptor transitions as in the case of Si-NCs, even if in the case of NWs, due to the fact that QC effects act only in the directions perpendicular to the growth axis, this reduction is much smaller. Only for edge-edge configuration valence band maximum and conduction band minimum are both localized on Si, whereas the impurity states are localized in the bands.

Table 3 DFT-LDA band gaps (in eV) for the pure H terminated Si-NW (<110> direction and diameter of 2.4 nm) and for different codoped P-B configurations.

Pure	B core-P core	B core-P edge	P core-B edge	B edge-P edge
0.97	0.91	0.81	0.80	0.96

4.3 Hexagonal Si nanowires

The theoretical and experimental investigation of novel phases in Si-NWs has attracted a huge interest in the last years [139–144]. In particular, Si-NWs showing the hexagonal-diamond (2H) phase have been the object of an intense study because of their potential of adding new functionalities to 3C Si-NWs. The electronic, optical and transport properties of 2H-Si-NWs [145–151] have been under scrutiny highlighting how this phase can offer a further degree of property modulation with respect to the versatility of 3C-Si-NWs. For example, it has been shown that 2H-Si-NWs are characterized by a more pronounced QC effect than 3C-Si-NWs and by a more enhanced optical absorption in the visible region [147]. For very small diameters, 2H-Si-NWs have a larger band gap with respect to 3C-Si ones, but the difference vanishes for diameters of the order of 4 nm and then it changes sign for larger diameters. For very large NWs, when QC effects become negligible, band gaps converge to the bulk value, that is 0.1-0.2 eV larger for 3C than for 2H. Indeed, differently from the 3C case, the band gap of 2H-Si-NWs is indirect for the smallest considered diameter, but it becomes direct for the other cases [147].

4.4 Doped hexagonal Si-NWs

Much less attention have been dedicated instead to the behaviour of dopants in 2H-Si-NWs. In a recent study [151] we performed ab initio DFT calculations to describe the properties of p-type and n-type dopants, located at the innermost sites, in 2H-Si-NWs comparing our results with those obtained for 3C-Si-NWs. All the surface dangling bonds are saturated by H atoms. Our findings for the middle and large diameters NWs (beyond the QC regime) can be summarized as follows: i) p-dopants have a lower formation energy when they are in 2H wires with respect to 3C ones, ii) n-type dopants, in first approximation, do not show any preference of phase. The origin of this different behaviour was ascribed to the different symmetry that is induced when a dopant is inserted in one specific phase. While p-type dopants preserve the C_{3V} symmetry of the host 2H lattice, n-type dopants show a clear tendency to occupy T_d lattice sites.

Here, we expand on our previous results by investigating the structural and electronic properties of group III and V dopants in ultrathin Si-NWs (with diameter of 2 nm).

We performed ab initio DFT calculations whose details are the same of Ref. [151].

Table 4 The calculated formation energy (E_{form}) (in eV) for group III (B, Al, Ga) and V (N, P, As) impurities in 3C-Si- and 2H-Si-NWs.

Group	Impurity	3C-NWs	2H-NWs
	B	-6.338	-6.230
III	Al	-2.609	-2.637
	Ga	-1.727	-1.754
	N	-4.201	-4.158
V	P	-5.059	-4.908
	As	-2.541	-2.423

As a first step, in order to investigate the structural stability of an impurity in one phase with respect to the other, we performed calculations of FE, within the scheme reported in Ref.[151]. Results of these calculations are reported in Table 4. The table clearly shows that, for both group III and V impurities, the difference in the FE between the two phases does not exceed 0.1 eV. Though the stability of impurities is slightly larger in the cubic phase, this means that there is not a clear preference of one phase with respect to the other one. This finding is in contrast to what was found in the case of middle and large diameter NWs[151]. This different behaviour can be related to the different structural reorganization around the impurity that one can observe in ultrathin NWs. While in the bulk system and large diameter NWs the host crystal, together with its symmetry, may favor or not the stability of a given impurity, in the case of a small NW the major degree of geometrical relaxation is an ideal chemical environment for all the types of dopants. In other words, each impurity can find its structural stability regardless of the phase. This is more evident if one looks at the first neighbours distance around the impurity after relaxation reported in Table 5 and 6.

Interestingly, the local symmetry around the impurity in an ultrathin NW does not change too much from one phase to the other. This is in contrast with respect to what we found in the case of large diameter NWs in which the rigidity of the host lattice has a much pronounced influence on determining the dopant symmetry. When the size of the NW shrinks down to few nm, the possibility for Si atoms to accommodate stress is much larger in both the phases and hence the role of the symmetry of the host lattice is less pronounced. This is the reason why, as in the case of Si-NCs, group III atoms, have a C_{3V} symmetry (three short and one longer bond length with first neighbours) in both 3C- and 2H-Si-NWs (see Table 5) while group V atoms present, independently from the phase, the T_d configuration (the four bond lengths are practically the same, see Table 6, with the exception of N, the smallest impurity).

Calculations of the electronic structure have been done only for B and P impurities, which are the most common dopants for both 3C- and 2H-NWs. Results of band structure calculations are reported in Fig. 6 and Fig. 7. With respect to the band structures of the corresponding undoped NWs[147] we note the presence of the impurity states near the band edges (B atom state is located near the valence band, that related to the P atom near the conduction band). Comparing the to plots for the doped structures,

Table 5 The nearest neighbour distances to the first neighbouring atoms of impurities for group III impurities in 3C-Si- and 2H-Si-NWs. For 2H systems, the first three bond lengths corresponds to bonds between atoms in the basal plane of the hexagonal cell. The fourth bond length is instead the one along the c direction.

Impurity	NW structure	Bond length (Å)
	Cubic-diamond (3C)	2.048
		2.048
		2.048
		2.055
B		
	Hexagonal-diamond (2H)	2.052
		2.052
		2.052
		2.063
	Cubic-diamond (3C)	2.394
		2.394
		2.394
		2.424
Al		
	Hexagonal-diamond (2H)	2.413
		2.414
		2.414
		2.397
	Cubic-diamond (3C)	2.396
		2.396
		2.396
		2.444
Ga		
	Hexagonal-diamond (2H)	2.420
		2.421
		2.421
		2.395

there are few interesting differences that can be pointed out: i) the impurity state in the 2H phase are always flatter than in the case of 3C, as a consequence of the more pronounced QC effect of the former, ii) the activation energy of the B dopant is larger in the case of 2H-Si-NW with respect to the 3C phase (70 meV to be compared with 163 meV, respectively). In the case of P we observed an opposite behaviour as the activation energy amounts to 180 meV in 2H-Si-NW to be compared with 95 meV calculated for 3C systems.

5 Conclusions

The properties of undoped and n- and p-doped Si-NCs and Si-NWs obtained through ab-initio calculations have been discussed. We showed that first-principle calculations can be a powerful tool for the understanding of the effects induced by substitutional doping on the structural, electronic and optical properties of free-standing and matrix-embedded Si nanostructures. The preferential positioning of the dopants and their effects on the structural properties with respect to the undoped case, as a function of the nanocrystals diameter and termination, have been characterized through total-energy considerations. The localization of the ac-

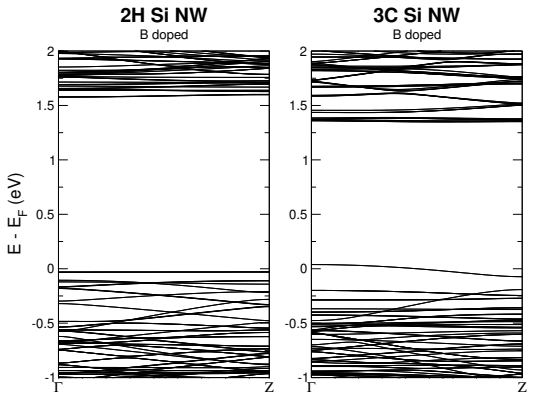

Fig. 6 Band structure of B doped 2H-Si-NWs (left) and B doped 3C-Si-NWs (right). The zero of the energy is set to the Fermi energy of the system.

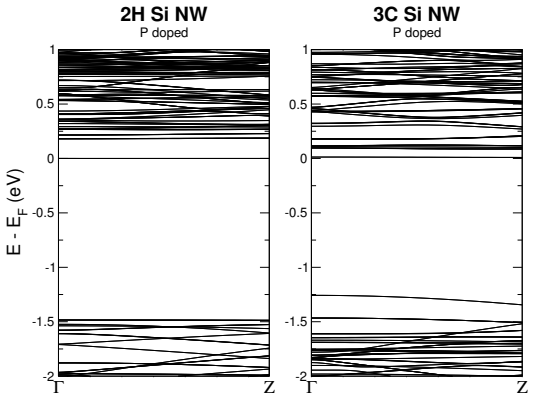

Fig. 7 Band structure of P doped 2H-Si-NWs (left) and P doped 3C-Si-NWs (right). The zero of the energy is set to the Fermi energy of the system.

Table 6 The nearest neighbour distances to the first neighbouring atoms of impurities for group V impurities in 3C-Si- and 2H-Si-NWs. For 2H systems, the first three bond lengths corresponds to bonds between atoms in the basal plane of the hexagonal cell. The fourth bond length is instead the one along the c direction.

Impurity	NW structure	Bond length (Å)
	Cubic-diamond (3C)	2.000
		2.004
		2.004
		2.005
N		
	Hexagonal-diamond (2H)	1.984
		1.984
		1.985
		2.057
	Cubic-diamond (3C)	2.332
		2.332
		2.333
		2.328
P		
	Hexagonal-diamond (2H)	2.345
		2.345
		2.346
		2.347
	Cubic-diamond (3C)	2.435
		2.439
		2.435
		2.427
As		
	Hexagonal-diamond (2H)	2.449
		2.449
		2.450
		2.444

ceptor and donor related levels in the band gap of the Si-NCs and Si-NWs, together with the impurity activation energy, have been discussed as a function of the nanostructures size. The dopant induced differences in the optical properties with respect to the undoped case have been presented. The role played by interface effects, orientation growth and phases has been outlined. Indeed we have studied the case of B and P codoped nanocrystals and nanowires showing that if carriers are perfectly compensated, the Si nanostructures undergo a minor structural distortion around the impurities inducing a significant decrease of the impurities formation energies with respect to the single doped case. Due to codoping, additional peaks are introduced in the absorption spectra, giving rise to a size- and dopant localization- dependent red-shift of the optical spectra. These results give a strong indication that with doping it is possible to efficiently tune the optical properties of silicon nanostructures.

Conflicts of interest

There are no conflicts to declare.

Acknowledgements

S.O. acknowledges support/funding from University of Modena and Reggio Emilia under project "FAR2017INTERDISC". M.A. greatly acknowledges the Transnational Access Programme of the HPC-EUROPA3 (project HPC17PB9IZ). Part of the high-performance computing (HPC) resources for this project were granted by the Institut du developpement et des ressources en informatique scientifique (IDRIS) under the allocation A0040910089 via GENCI (Grand Equipement National de Calcul Intensif). This work was supported by the ANR HEXSIGE project (ANR-17-CE030-0014-01) of the French Agence Nationale de la Recherche. We also acknowledge financial support by the Ministerio de Economía, Industria y Competitividad (MINECO) and MICIU (Ministerio de Ciencia y Universidades) under Grants FEDER-MAT2017-90024-P, FIS2015-64886-C5-4-P and PGC2018-096955-B-C44-P, the Severo Ochoa Centres of Excellence Program under Grant SEV-2015-0496, the Generalitat de Catalunya under Grants 2017 SGR 1506.

Notes and references

1 L. T. Canham, *Appl. Phys. Lett.*, 1990, **57**, 1046–1048.

2 H. Takagi, H. Ogawa, Y. Yamazaki, A. Ishikazi and T. Nakagiri, *Appl. Phys. Lett.*, 1990, **56**, 2379–2381.

3 S. Ossicini, F. Bernardini and A. Fasolino, *Phys. Rev. Lett.*, 1994, **72**, 1044–1047.

4 O. Bisi, S. Ossicini and L. Pavesi, *Surface Sci. Rep.*, 2000, **38**, 1–126.

5 R. Rurali, *Rev. Mod. Phys.*, 2010, **82**, 427–449.

6 M. Amato, M. Palummo, R. Rurali and S. Ossicini, *Chem. Rev.*, 2014, **114**, 1371–1412.

7 A. R. Goñi, L. R. Muniz, J. S. Reparaz, M. I. Alonso, M. Garriga, A. F. Lopeandia, J. Rodríguez-Viejo, J. Arbiol and R. Rurali, *Phys. Rev. B*, 2014, **89**, 045428.

8 I. Pelant, *Phys. Status Solidi A*, 2011, **208**, 625–630.

9 F. Priolo, F. Gregorkiewicz, M. Galli and T. F. Krauss, *Nature Nanotechnol.*, 2014, **1**, 19–32.

10 D. Jurbergs, E. Rogojina, L. Mangolini and U. Kortshagen, *Appl. Phys. Lett.*, 2006, **88**, 233116.

11 L. Pavesi, L. Dal Negro, C. Mazzoleni, G. Franzó and F. Priolo, *Nature*, 2000, **408**, 440–444.

12 L. Dal Negro, M. Cazzanelli, L. Pavesi, S. Ossicini, D. Pacifici, G. Franzó, F. Priolo and F. Iacona, *Appl. Phys. Lett.*, 2003, **82**, 4636–4638.

13 J. Ruan, P. M. Fauchet, L. Dal Negro, M. Cazzanelli and L. Pavesi, *Appl. Phys. Lett.*, 2003, **83**, 5479–5481.

14 E. Degoli, R. Guerra, F. Iori, R. Magri, I. Marri, O. Pulci, O. Bisi and S. Ossicini, *C. R. Phys.*, 2009, **10**, 575–586.

15 M. C. Beard, K. P. Knutsen, P. Yu, J. M. Luther, Q. Song, W. K. Metzger, R. J. Ellingson and A. J. Nozik, *Nano Lett.*, 2007, **7**, 2506–2512.

16 D. Timmermann, L. Izeddin, P. Stallinga, I. N. Yassevich and T. Gregorkiewicz, *Nature Photon.*, 2008, **2**, 105–109.

17 M. T. Trinh, R. Limpens, W. D. A. M. de Boer, J. M. Schins, L. D. A. Siebbeles and T. Gregorkiewicz, *Nature Photon.*, 2012, **6**, 316–321.

18 M. Govoni, I. Marri and S. Ossicini, *Phys. Rev. B*, 2011, **84**, 075215.

19 M. Govoni, I. Marri and S. Ossicini, *Nature Photon.*, 2012, **6**, 672–679.

20 I. Marri, M. Govoni and S. Ossicini, *J. Am. Chem. Soc.*, 2014, **136**, 13257–13266.

21 I. Marri, M. Govoni and S. Ossicini, *Beilstein J. Nanotech.*, 2015, **6**, 343–352.

22 I. Marri, M. Govoni and S. Ossicini, *Solar Energy Materials & Solar Cells*, 2016, **145**, 162–169.

23 J. D. Holmes, K. J. Ziegler, R. C. Doty, L. E. Pell, K. P. Johnston and B. A. Korgel, *J. Am. Chem. Soc.*, 2001, **123**, 3743–3748.

24 J. G. C. Veinot, *Chem. Commun.*, 2006, 4160–4168.

25 M. L. Mastronardi, F. Maier-Flaig, D. Faulkner, E. J. Henderson, C. Küble, U. Lemmer and G. A. Ozin, *Nano Lett.*, 2012, **12**, 337–342.

26 C. M. Hessel, D. Reid, M. G. Panthani, M. R. Rasch, B. W. Goodfellow, J. W. Wei, H. Fujii, V. Akhavan and B. A. Korgel, *Chem Mat.*, 2012, **24**, 393–401.

27 L. Mangolini, *J. Vac. Sci. Technol. B*, 2013, **31**, 020801.

28 O. Wolf, M. Dasog, Z. Yang, I. Balberg, J. C. G. Veinot and O. Millo, *Nano Lett.*, 2013, **13**, 2516–2521.

29 M. Dasog, G. B. De Los Reyes, L. V. Titova, F. Hegmann and J. G. C. Veinot, *ACS Nano*, 2014, **8**, 9636–9648.

30 K. Dohnalová, T. Gregorkiewicz and K. Kůsová, *J. Phys.: Condens. Matter*, 2014, **26**, 173201.

31 Y. Yu, R. C. E, R. Schaller and B. A. Korgel, *Langmuir*, 2015, **31**, 6886–6893.

32 D. Kim, J. M. Zuidema, J. Kang, Y. Pan, L. Wu, D. Warther, B. Arkles and M. J. Sailor, *J. Am. Chem. Soc.*, 2016, **138**, 15106–15109.

33 S. Ossicini, L. Pavesi and F. Priolo, *Springer Tracts in Modern Physics*, 2003, **194**, 1–282.

34 D. V. Talapin, J. S. Lee, M. V. Kovalenko and E. V. Shevchenko, *Chem. Rev.*, 2010, **110**, 389–458.

35 D. P. Puzzo, E. J. Henderson, M. G. Helander, Z. Wang, G. A. Ozin and Z. Lu, *Nano Lett.*, 2011, **11**, 1585–1590.

36 M. Dasog, J. Kehrle, B. Rieger and J. C. G. Veinot, *Angew. Chem. Int. Ed.*, 2016, **55**, 2322–2339.

37 N. Daldosso and L. Pavesi, *Laser & Photon. Rev.*, 2009, **3**, 508–534.

38 L. Kriachtchev, S. Ossicini, F. Iacona and F. Gourbilleau, *Int. J. Photoen.*, 2012, 872576.

39 R. Sinelnikov, M. Dasog, J. Beamish, A. Meldrum and J. C. G. Veinot, *ACS Photonics*, 2017, **4**, 1920–1929.

40 S. V. Makarov, M. I. Petrov, U. Zywietz, V. A. Milichko, D. A. Zuev, N. Lopanitsyna, A. Kuksin, I. Mukhin, G. Zograf, E. Ubyivovk, D. Smirnova, S. Starikov, B. N. Chichkov and Y. S. Kivshar, *Nanolett.*, 2017, **17**, 3914–3918.

41 M. A. Green, *Prog. Photovolt: Res. Appl.*, 2001, **9**, 123–135.

42 A. J. Nozik, *Nano Lett.*, 2010, **10**, 2735–2741.

43 T. Claudio, N. Stein, D. G. Stroppa, B. Klobes, M. M. Koz,

P. Kudejova, N. Petermann, H. Wiggers, G. Schierning and R. P. Hermann, *Phys. Chem. Chem. Phys.*, 2014, **16**, 25701–25709.

44 J.-H. Park, L. Gu, G. von Maltzahn, E. Ruoslahti, S. N. Bhatia and M. J. Sailor, *Nat. Mat.*, 2009, **8**, 331–336.

45 L. Gu, D. J. Hall, Z. Qin, E. Anglin, J. Joo, D. J. Mooney, S. B. Howell and M. J. Sailor, *Nat. Commun.*, 2013, **4**, 2326.

46 L. T. Canham, *Nanomedicine*, 2013, **8**, 1573–1576.

47 J. Joo, X. Liu, V. R. Kotamrju, E. Ruoslahti, Y. Nam and M. J. Sailor, *ACS Nano*, 2015, **9**, 6233–6241.

48 L. Ostrovska, A. Broz, A. Fucikova, T. Belinova, H. Sugimoto, T. Kanno, M. Fujii, J. Valenta and M. Hubalek Kabalcova, *RSC Advances*, 2016, **6**, 63403–63413.

49 B. F. P. McVey, S. Prabakar, J. J. Goodig and R. D. Tilley, *ChemPlusChem*, 2017, **82**, 60–73.

50 Y. Li, F. Qian, J. Xiang and C. M. Lieber, *Mat. Today*, 2006, **9**, 18–27.

51 V. Schmidt, J. V. Wittermann and U. Gösele, *Chem. Rev.*, 2010, **110**, 361–388.

52 Y. Wang, T. Wang, P. Da, M. Xu, H. Wu and G. Zheng, *Adv. Mat.*, 2013, **25**, 5177–5195.

53 M. Bruno, M. Palummo, A. Marini, R. Del Sole and S. Ossicini, *Phys. Rev. Lett.*, 2007, **98**, 036807.

54 M. Amato and R. Rurali, *Progress in Surface Science*, 2016, **91**, 1–28.

55 A. G. Cullis, L. T. Canham and P. D. J. Calcott, *J. Appl. Phys.*, 1997, **82**, 909–965.

56 G. Polisski, D. Kovalev, G. Dollinger, T. Sulima and F. Koch, *Physica B*, 1999, **273-274**, 951–954.

57 M. Fujii, Y. Yamaguchi, Y. Takase, K. Ninomiya and S. Hayashy, *Appl. Phys. Lett.*, 2005, **87**, 211919.

58 B. L. Oliva-Chatelain, T. M. Ticich and A. R. Barron, *Nanoscale*, 2016, **8**, 1733–1745.

59 E. Arduca and M. Perego, *Materials Science in Semiconductor Processing*, 2017, **62**, 156–170.

60 I. Marri, S. Ossicini and E. Degoli, *Progr. Surf. Sci.*, 2017, **92**, 3705–3748.

61 G. M. Credo, M. D. Mason and S. K. Buratto, *Appl. Phys. Lett.*, 1999, **74**, 1978–1981.

62 P. Hohenberg and Kohn, *Phys. Rev. B*, 1964, **136**, 864–871.

63 W. Kohn and L. J. Sham, *Phys. Rev. A*, 1965, **140**, 1133–1138.

64 L. Hedin, *Phys. Rev. A*, 1965, **139**, 796.

65 G. Onida, L. Reining and A. Rubio, *Rev. Mod. Phys.*, 2002, **74**, 601–659.

66 F. Iori, E. Degoli, R. Magri, I. Marri, G. Cantele, D. Ninno, F. Trani, O. Pulci and S. Ossicini, *Phys. Rev. B*, 2007, **76**, 085302.

67 M. Bruno, M. Palummo, A. Marini, R. Del Sole, V. Olevano, A. N. Kholod and S. Ossicini, *Phys. Rev. B*, 2005, **72**, 153310.

68 M. Luppi and S. Ossicini, *Phys. Rev. B*, 2005, **71**, 035340.

69 R. Guerra, I. Marri, R. Magri, L. Martin-Samos, O. Pulci, E. Degoli and S. Ossicini, *Phys. Rev. B*, 2009, **79**, 155320.

70 R. Guerra, I. Marri, R. Magri, L. Martin-Samos, O. Pulci, E. Degoli and S. Ossicini, *Superl. Microstr.*, 2009, **46**, 246–252.

71 P. Giannozzi, S. Baroni, N. Bonini, M. Calandra, R. Car, C. Cavazzoni, D. Ceresoli, G. L. Chiarotti, M. Cococcioni, J. Dabo, A. Dal Corso, S. Fabris, G. Fratesi, S. de Gironcoli, R. Gebauer, U. Gerstmann, C. Gougoussis, A. Kokalj, M. Lazzeri, L. Martin-Samos, N. Marzari, F. Mauri, R. Mazzarello, S. Paolini, A. Pasquarello, L. Paulatto, C. Sbraccia, S. Scandolo, G. Sclauzero, P. Seitsonen, A. Smogunov, P. Umari and R. M. Wentzcovitch, *J. Phys.: Condens. Matter*, 2009, **21**, 395502.

72 P. Giannozzi, O. Andreussi, T. Brumme, O. Bunau, M. B. Nardelli, M. Calandra, R. Car, C. Cavazzoni, D. Ceresoli, M. Cococcioni *et al.*, *J. Phys. Condens. Matter*, 2017, **29**, 465901.

73 J. M. Soler, E. Artacho, J. D. Gale, A. García, J. Junquera, P. Ordejón and D. Sánchez-Portal, *J. Phys. Cond. Matt.*, 2002, **14**, 2745–2779.

74 X. Gonze, J.-M. Beuken, R. Caracas, F. Detraux, M. Fuchs, G.-M. Rignanese, L. Sindic, M. Verstaete, G. Zerah, F. Jollet, M. Torrent, A. Roy, M. Mikami, P. Ghosez, J.-P. Raty and D. C. Allan, *Comput. Mater. Sci.*, 2002, **25**, 478–492.

75 G. Kresse and J. Furthmüller, *Comput. Mater. Sci.*, 1996, **6**, 15–50.

76 D. Sangalli, A. Ferretti, H. Miranda, C. Attaccalite, I. Marri, E. Cannuccia, P. Melo, M. Marsili, F. Paleari, A. Marrazzo *et al.*, *J. Phys. Condens. Matter*, 2019, **31**, 325902.

77 Y. Q. Wang, S. Smirani and G. G. Ross, *Nano Lett.*, 2004, **4**, 2041–2045.

78 R. Guerra, E. Degoli and S. Ossicini, *Phys. Rev. B*, 2009, **80**, 155332.

79 L. E. Ramos, E. Degoli, G. Cantele, S. Ossicini, D. Ninno, J. Furthmüller and F. Bechstedt, *J. Phys.: Condens. Matter*, 2007, **19**, 466211.

80 L. E. Ramos, E. Degoli, G. Cantele, S. Ossicini, D. Ninno, J. Furthmüller and F. Bechstedt, *Phys. Rev. B*, 2008, **78**, 235310.

81 S. Kim, M. C. Kim, S. H. Choi, K. J. Kim, H. N. Hwang and C. C. Hwang, *Appl. Phys. Lett.*, 2007, **92**, 103113.

82 M. V. Wolkin, J. Jorne, J. M. Fauchet, G. Allan and C. Delerue, *Phys. Rev. Lett.*, 1999, **82**, 000197.

83 L. Dorigoni, O. Bisi, F. Bernardini and S. Ossicini, *Phys. Rev. B*, 1996, **53**, 4557–4564.

84 M. Sykora, L. Mangolini, R. D. Schaller, U. Kortshagen, D. Jurbergs and V. I. Klimov, *Phys. Rev. Lett.*, 2008, **100**, 067401.

85 M. Luppi and S. Ossicini, *J. Appl. Phys.*, 2003, **94**, 2130–2132.

86 N. Daldosso, M. Luppi, S. Ossicini, E. Degoli, R. Magri, G. Dalba, D. Fornasini, R. Grisenti, F. Rocca, L. Pavesi, S. Boninelli, F. Priolo, C. Spinella and F. Iacona, *Phys. Rev. B*, 2003, **68**, 085327.

87 Z. Zhou, L. Brus and R. Friesner, *Nano Lett.*, 2003, **3**, 163–167.

88 R. Guerra and S. Ossicini, *Phys. Rev. B*, 2010, **81**, 245307.

89 G. Seguini, C. Castro, S. Schamm-Chardon, G. BenAssayag, P. Pellegrino and M. Perego, *Appl. Phys. Lett.*, 2013, **103**, 023103.

90 D. V. Melnikov and J. R. Chelikowsky, *Phys. Rev. Lett.*, 2004, **92**, 046802.

91 G. Cantele, E. Degoli, E. Luppi, R. Magri, D. Ninno, G. Jadonisi and S. Ossicini, *Phys. Rev. B*, 2005, **72**, 113303.

92 S. Ossicini, E. Degoli, F. Iori, E. Luppi, R. Magri, G. Cantele, F. Trani and D. Ninno, *Appl. Phys Lett.*, 2005, **87**, 173120.

93 G. M. Dalpian and J. R. Chelikowsky, *Phys. Rev. Lett.*, 2006, **96**, 226802.

94 T. L. Chan, M. L. Tiago, E. Kaxiras and J. R. Chelikowsky, *Nano Lett*, 2008, **8**, 596–600.

95 D. J. Norris, A. L. Efros and S. C. Erwin, *Science*, 2008, **319**, 1766–1779.

96 J. Li, S. H. Wei, S. S. Li and J. B. Xia, *Phys. Rev. B*, 2008, **77**, 113304.

97 J. R. Chelikowsky, M. M. G. Alemany, T. L. Chan and G. M. Dalpian, *Rep. Prog. Phys.*, 2011, **74**, 046501.

98 S. B. Zhang and J. E. Northrup, *Phys. Rev. Lett.*, 1991, **67**, 2339–2342.

99 J. E. Northrup and S. B. Zhang, *Phys. Rev. B*, 1993, **47**, 6791–6794.

100 C. Freysoldt, B. Grabowski, T. Hickel, J. Neugebauer, G. Kresse, A. Janotti and C. G. Van de Walle, *Rev. Mod. Phys.*, 2014, **86**, 253–305.

101 J. H. Eom, T. L. Chan and J. R. Chelikowsky, *Solid State Commun.*, 201, **150**, 130–132.

102 X. D. Pi, R. Gresback, R. W. Liptak, S. A. Campbell and U. Kortshagen, *Appl. Phys. Lett.*, 2008, **92**, 123102.

103 H. Sugimoto, M. Fujii, M. Fukuda, K. Imakita and S. Hayashi, *J. Appl. Phys.*, 2011, **110**, 063528.

104 N. J. Kramer, K. S. Schramke and U. R. Kortshagen, *Nano Lett.*, 2015, **15**, 5597–5603.

105 R. Guerra and S. Ossicini, *J. Am. Chem. Soc.*, 2014, **136**, 4404–4409.

106 M. Perego, G. Seguini and Fanciulli, *Surf. Interface Anal.*, 2013, **45**, 386–389.

107 M. Perego, G. Seguini, E. Arduca, J. Frascaroli, D. De Salvador, M. Mastromatteo, A. Carnera, G. Nicotra, M. Scuderi, C. Spinella, G. Impellizzeri, C. Lenardi and E. Napolitani, *Nanoscale*, 2015, **7**, 14469–14475.

108 M. Xie, D. Li, L. Chen, F. Wang, X. Zhu and D. Yang, *Appl. Phys. Lett.*, 2013, **102**, 123108.

109 K. Nomoto, H. Sugimoto, A. Breen, A. V. Ceguerra, T. Kanno, S. P. Ringer, I. Perez-Würfl, G. Conibeer and M. Fujii, *J. Phys. Chem. C*, 2016, **120**, 17845–17852.

110 R. Khelifi, D. Mathiot, R. Gupta, D. Muller, M. Roussel and S. Duguay, *Appl. Phys. Lett.*, 2013, **102**, 013116.

111 M. Frégnaux, R. Khelifi, D. Muller and D. Mathiot, *J. Appl. Phys.*, 2014, **116**, 143505.

112 M. Fujii, Y. Yamaguchi, Y. Takase, K. Ninomiya and S. Hayashi, *Appl. Phys. Lett.*, 2004, **85**, 1158–1160.

113 T. Nakamura, S. Adachi, M. Fujii, H. Sugimoto, K. Miura and S. Yamamoto, *Phys. Rev. B*, 2015, **91**, 165424.

114 N. X. Chung, R. Limpens, A. Lesage, M. Fujii and T. Gregorkiewicz, *Phys. Status Solidi A*, 2016, **11**, 2863–2866.

115 D. Li, Y. Jiang, Z. P, D. Shan, J. Xu, W. Li and K. Chen, *Appl. Phys. Lett.*, 2017, **110**, 233105.

116 O. Ashkenazi, D. Azulay, I. Balberg, S. Kano, H. Sugimoto, M. Fujii and O. Millo, *Nanoscale*, 2017, **9**, 17884–17892.

117 H. Sugimoto, M. Yamamur, R. Rujii and M. Fujii, *Nano Lett.*, 2018, **18**, 7282–7288.

118 V. Mulloni, P. Bellutti and L. Vanzetti, *Surf. Sci.*, 2005, **585**, 137–143.

119 E. Sun, F.-H. Su, C.-H. Chen, H.-L. Tsai, J.-R. Yang and M.-J. Chen, *J. Lumin.*, 2010, **130**, 1485–1488.

120 D. Puglia, G. Sombrio, R. dos Reis and H. Boudinov, *Mat. Res. Express*, 2018, **5**, 036201.

121 R. Demoulin, M. Roussel, S. Duguay, D. Muller, D. Mathiot, P. Pareige and E. Talbot, *J. Phys, Chem. C*, 2019, **123**, 7381–7389.

122 M. Palummo, C. Hogan and S. Ossicini, *Phys. Chem. Chem. Phys.*, 2015, **17**, 29085–29089.

123 D. Ma, C. Lee, F. Au, S. Tong and S. Lee, *Science*, 2003, **299**, 1874–1877.

124 H. Peelaers, B. Partoens and F. M. Peeters, *Nano Lett.*, 2006, **6**, 2781–2784.

125 B. Schoeters, O. Leenaerts, G. Pourtois and B. Partoens, *J. Appl. Phys.*, 2015, **118**, 104306.

126 M. V. Fernández-Serra, C. Adessi and X. Blase, *Phys. Rev. Lett.*, 2006, **96**, 166805.

127 M. Diarra, Y.-M. Niquet, C. Delerue and G. Allan, *Phys. Rev. B*, 2007, **75**, 045301.

128 C. R. Leao, A. Fazzio and A. J. R. da Silva, *Nano Lett.*, 2008, **8**, 1866–1871.

129 R. Rurali and X. Cartoixà, *Nano Lett.*, 2009, **9**, 975–979.

130 M. Palummo, F. Iori, R. Del Sole and S. Ossicini, *Superlatt. Microstruct.*, 2009, **46**, 234–239.

131 R. Kagimura, R. W. Nunes and H. Chacham, *Phys. Rev. Lett.*, 2005, **95**, 115502.

132 N. Fukata, *Adv. Mat.*, 2009, **21**, 2829–2832.

133 E. Koren, N. Berkovitch and Y. Rosenwaks, *Nano Lett.*, 2010, **10**, 1163–1167.

134 S. G. Pavlov, R. Eichholz, N. V. Abrisimov, B. Redlich and H. W. Hubers, *Appl. Phys. Lett.*, 2011, **98**, 061102.

135 N. Fukata, J. Kaminaga, R. Takiguchi, R. Rurali, M. Dutta and K. Murakami, *J. Phys. Chem. C*, 2013, **117**, 20300–20307.

136 L. Yang, L. Zhihong, L. Xiaoxiang, S. Zhihua, W. Yanan, L. Rui, W. Dunwei, J. Jie, L. Joon Hwan, W. Haiyan, Y. Qingkai and B. Jiming, *Nanoscale*, 2015, **7**, 1601–1605.

137 N. Fukata, J. Chen, T. Sekiguchi, S. Matsuhita, T. Oshima, N. Uchida, K. Murakami, T. Tsurui and S. Ito, *Appl. Phys. Lett.*, 2008, **93**, 203106.

138 M. Amato, M. Palummo, R. Rurali and S. Ossicini, *J. Phys. D: Appl. Phys.*, 2014, **47**, 394013.

139 L. Vincent, G. Patriarche, G. Hallais, C. Renard, C. GardÃĺs, D. Troadec and D. Bouchier, *Nano Lett.*, 2014, **14**, 4828–4836.

140 L. Vincent, D. Djomani, M. Fakfakh, C. Renard, B. Belier, D. Bouchier and G. Patriarche, *Nanotechnology*, 2018, **29**, 125601.

141 H. I. T. Hauge, M. A. Verheijen, S. Conesa-Boj, T. Etzelstorfer, M. Watzinger, D. Kriegner, I. Zardo, C. Fasolato, F. Capitani, P. Postorino, S. Kölling, A. Li, S. Assali, J. Stangl and E. P. A. M. Bakkers, *Nano Lett.*, 2015, **15**, 5855–5860.

142 H. I. T. Hauge, S. Conesa-Boj, M. A. Verheijen, S. Koelling and E. P. A. M. Bakkers, *Nano Lett.*, 2017, **17**, 85–90.

143 J. Tang, J.-L. Maurice, F. Fossard, I. Florea, W. Chen, E. Johnson, M. Foldyna, L. Yu and P. R. i Cabarrocas, *Nanoscale*, 2017, **9**, 8113–8118.

144 Z. He, J.-L. Maurice, Q. Li and D. Pribat, *Nanoscale*, 2019, **11**, 4846–4853.

145 C. Rödl, T. Sander, F. Bechstedt, J. Vidal, P. Olsson, S. Laribi and J.-F. Guillemoles, *Phys. Rev. B*, 2015, **92**, 045207.

146 T. Kaewmaraya, L. Vincent and M. Amato, *J. Phys. Chem. C*, 2017, **121**, 5820–5828.

147 M. Amato, T. Kaewmaraya, A. Zobelli, M. Palummo and R. Rurali, *Nano Lett.*, 2016, **16**, 5694–5700.

148 F. Fabbri, E. Rotunno, L. Lazzarini, D. Cavalcoli, A. Castaldini, N. Fukata, K. Sato, G. Salviati and A. Cavallini, *Nano Lett.*, 2013, **13**, 5900–5906.

149 S. Dixit and A. K. Shukla, *J. Appl. Phys.*, 2018, **123**, 224301.

150 F. Fabbri, E. Rotunno, L. Lazzarini, N. Fukata and G. Salviati, *Sci. Rep.*, 2014, **4**, 3603.

151 M. Amato, S. Ossicini, E. Canadell and R. Rurali, *Nano Lett.*, 2019, **19**, 866–876.